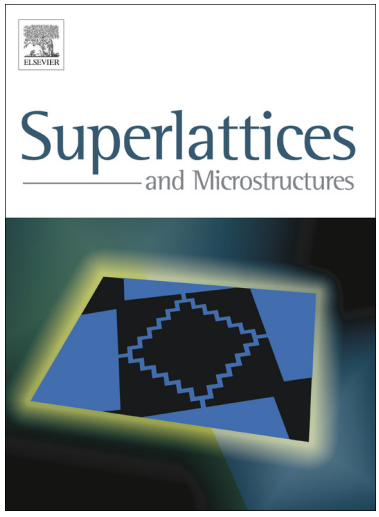


# Structural and optical properties of $ZnS/MgNb_2O_6$ heterostructures

L.P.S. Santos, L.S. Cavalcante, M.T. Fabbro, H. BeltránMir, E. Cordoncillo, J. Andrés, E. Longo

PII: S0749-6036(14)00475-3
DOI: http://dx.doi.org/10.1016/j.spmi.2014.12.007
Reference: YSPMI 3524

To appear in: *Superlattices and Microstructures*

Received Date: 10 September 2014
Revised Date: 8 December 2014
Accepted Date: 9 December 2014

Please cite this article as: L.P.S. Santos, L.S. Cavalcante, M.T. Fabbro, H. BeltránMir, E. Cordoncillo, J. Andrés, E. Longo, Structural and optical properties of $ZnS/MgNb_2O_6$ heterostructures, *Superlattices and Microstructures* (2014), doi: http://dx.doi.org/10.1016/j.spmi.2014.12.007

# Structural and optical properties of $ZnS/MgNb_2O_6$ heterostructures

L.P.S. Santos[a], L.S. Cavalcante[b], M.T. Fabbro[c,d], H. Beltrán Mir[c], E. Cordoncillo[c], J. Andrés[e], E. Longo[f]

[a]*Instituto Federal do Maranhão, Departamento de Química/INCTMN, Campus Monte Castelo, Av. Getúlio Vargas, 04, CEP. 65030-005, São Luís-MA, Brazil*

[b]*Universidade Estadual do Piauí, CCN-DQ-GERATEC, João Cabral, N. 2231, P.O. Box 381, CEP: 64002-150, Teresina-PI, Brazil*

[c]*Universitat Jaume I, Departamento de Química Inorgánica y Orgánica, Campus del Riu Sec, E-12071, Castellón, Spain*

[d]*Universidade Federal de São Carlos, Departamento de Química, CDMF/INCTMN, Via Washington Luiz, Km 235, P.O. Box 676, CEP. 13565-905, São Carlos-SP, Brazil*

[e]*Universitat Jaume I, Departamento de Química Física y Analítica, Campus del Riu Sec, E-12071, Castellón, Spain*

[f]*Universidade Estadual Paulista, Instituto de Química, CDMF/INCTMN, Rua Francisco Degni, 55, CEP. 14800-900, Araraquara-SP, Brazil*

## Abstract

In this letter, we report a simple and efficient synthetic procedure where the first step is a coprecipitation/calcination method used to obtain magnesium niobate $MgNb_2O_6$ (MN) nanocrystals and in the second stage a microwave assisted hydrothermal method (MAH) is employed to synthesize zinc sulfide (ZnS) nanocrystals and ZnS/MN heterostructures. These heterostructures were characterized by X-ray diffraction (XRD), micro-Raman (MR) spectroscopy, field emission scanning electron microscopy (FE-SEM), transmission electron microscopy (TEM), high-resolution TEM (HR-TEM), selected area electron diffraction (SAED), energy dispersive X-ray spectrometry (EDX). XRD patterns and MR spectra indicate that MN and ZnS nanocrystals have an orthorhombic and cubic structure, respectively. FE-SEM, TEM and HR-TEM images proved the presence of aggregated MN nanocrystals, ZnS nanocrystals and the presence of ZnS nanocrystals on the surface of MN nanocrystals. Their optical properties were investigated by ultraviolet−visible spectroscopy (UV-vis) and photoluminescence (PL) measurements at room temperature. ZnS/MN heterostructures show a decrease in the values for the optical band gap with respect to both components. The presence of the ZnS nanocrystals in this heterostructure promotes a high intense PL emission.

*Keywords:* $ZnS/MgNb_2O_6$; Chemical synthesis; Heterostructures; Band gap; Photoluminescence.

*Tel: +55 16 3351 8214, Mob: +55 16 99199 4343. Email address: presleyserejo@gmail.com (L.P.S. Santos*)

*Preprint revised to Superlattices and Microstructures* *September 08, 2014*

## 1. Introduction

Ceramic samples based on binary niobates with general formula [(M)$Nb_2O_6$] (where: M = $Ca^{2+}$, $Mg^{2+}$, or a transition metal) exhibit a crystalline columbite-type orthorhombic structure at room temperature [1-2]. There is a growing interest in this material because this ceramic oxide presents an interesting electronic structure [3-4]. In particular, magnesium niobate $MgNb_2O_6$ (MN) nanoparticles show excellent dielectric and optical properties [5-8]. It has been widely used as a precursor in the synthesis of $Pb(Mg_{1/3}Nb_{2/3})O_3$ (PMN) (single-phase) and PMN-$PbTiO_3$ (PT) solid solutions. The synthesis of zinc sulfide (ZnS) nanoparticles has been the focus of recent scientific research due to their important nonlinear optical properties, luminescence, and other important physical and chemical properties [9-10].

The ability to synthetize semiconductor/semiconductor heterostructures with enhanced luminescence and conductive properties is a challenging problem [11-12]. The photoluminescence behavior of nanostructured materials depends not only on the structure but also is controlled by surface chemical bonding and optical transitions in the region of the surface/interface [13-15]. MN is a luminescent material with energy gap of 3.6 eV, while ZnS can presents a zinc-blende and/or wurtzite phases, with energy gaps of 3.7 eV and 3.8 eV, respectively.

Figure 1(a,b) shows a schematic representation of the $MgNb_2O_6$ and ZnS crystals (1×1×1) unit cells with their respective clusters.

**<Fig. 1(a,b)>**

Fig. 1(a) illustrates a unit cell for MN crystals with a columbite-type orthorhombic structure, a space group of (*Pbcn*) and point-group symmetry ($D_{2h}$). In this unit cell, magnesium atoms (Mg) and niobium (Nb) atoms are coordinated to six oxygen (O) atoms which form distorted octahedral

$[MgO_6]/[NbO_6]$ clusters [16]. These octahedra are formed by 6-vertices, 6-faces and 12-edges. In addition, the MN crystals are characterized by an ionic character between the Mg–O bonds, while the Ti–O bonds present a covalent nature. Fig. 1(b) shows a unit cell for ZnS crystals with a sphalerite-type cubic structure, space group (F-43m) and point-group symmetry ($T_d$). In this unit cell, the zinc (Zn) atoms are coordinated to four oxygen atoms forming the polyhedra with a tetrahedral configuration related to $[ZnS_4]$ clusters [17]. These tetrahedra are formed by the 4 vertices, 4 faces and 6 edges.

In this research, MN nanocrystals were obtained by a coprecipitation/calcination method and in the second stage a microwave assisted hydrothermal method was employed to synthesize zinc sulfide (ZnS) nanocrystals and ZnS/MN heterostructures in the order to investigate the optical and structural properties of these novel heterostructures. Based on the experimental results, a plausible mechanism for a relationship between optical properties and order-disorder effects is proposed.

## 2. Experimental details

### 2.1. *Synthesis of $MgNb_2O_6$ nanocrystals*

$MgNb_2O_6$ nanocrystals were synthesized by the coprecipitation/calcination method. First, a stoichiometric amount of niobium chloride ($NbCl_5$, 99.9%, Aldrich) was dissolved in deionized water and stirred at 40 ºC until total solution was obtained, with a $NbCl_5$:$H_2O$ molar ratio was 1:1. The above solution was mixed with another solution containing magnesium acetate (99%, Vetec, $Mg(OAc)_2$:$H_2O$ molar ratio 1:1) to obtain a final solution with a Mg:Nb molar ratio of 1:2. Ammonium hydroxide ($NH_4OH$, 30%, Synth) was slowly added to the above solution dropwise and this solution was stirred at 70 ºC until a gel was formed. The gel was dried at 60 ºC for 12 h in an oven. The resulting white and dry powder was then ground with an agate pestle. This powder was calcined between 700 °C and 1000 ºC for 1 h in an electric furnace for crystallization of MN nanocrystals.

### 2.2. *Synthesis of ZnS/$MgNb_2O_6$ heterostructure*

ZnS nanocrystals were obtained and the capping process of the ZnS layer on the MN nanocrystals was accomplished MAH method. ZnS nanoparticles were synthesized using a stoichiometric amount of zinc acetate (99.99%, Aldrich, $Zn(OAc)_2$:$H_2O$ molar ratio of 1:1) was dissolved in deionized water and ammonium hydroxide solution was added drop wise until a clear solution was obtained (solution 1). Thioacetamide ($CH_3CSNH_2$, 99.0%, Aldrich) was separately dissolved into deionized water (solution 2). The thioacetamide:$H_2O$ molar ratio was 1:1. Under vigorous magnetic stirring, solution 2 was then quickly added to solution 1. The zinc solution and thioacetamide solution were prepared with a 1 to 1 mole ratio. The final solution was transferred to a teflon autoclave, which was sealed and placed inside MAH system (2.5 GHz, maximum power of 400 W, MW ETHOS ONE). The MAH was performed at 180 ºC for 1 h. The precipitate was collected on a filter, washed with deionized water, and dried at 60 ºC overnight. The same procedure previously described was employed for the synthesis of ZnS/MN heterostructure. MN (previously prepared by the homogeneous precipitate method) was added to the mixture of the solution 1 and solution 2. Then, the final solution was transferred into a Teflon autoclave. The MAH treatment was performed at 180 °C for 1 h. The precipitates were filtered and dried at 60 ºC for 12 h and the ZnS/MN heterostructure was obtained.

### 2.3. *Characterization*

The ZnS/MN heterostructure was structurally characterized by XRD in the 2θ range from 10º to 75º using Cu-Kα radiation (Rigaku-DMax/2500 PC). MR measurements were recorded using a Modular Raman Spectrometer (Horiba, Jobin Yvon), model RMS-550 with an Ar laser excitation at 514 nm and fibre-microscope. The morphology, microanalysis and size of nanoparticles and heterostructure were determined by TEM (JEOL / JEM-2100), coupled with an INCA Energy TEM 200 (Oxford) EDX and FE-SEM (Supra 35-VP, Carl Zeiss). UV-vis spectra were taken using a Varian spectrophotometer (Model Cary 5G) in the diffuse reflection mode. PL spectra were collected with a Thermal Jarrel Ash Monospec monochromator and a Hamamatsu R446

Photomultiplier. The 350.7 nm (2.57 eV) exciting wavelength of a krypton ion laser (Coherent Innova) was used with the output of the laser kept at 200 mW. All measurements were taken at room temperature.

## 3. Results and discussion

### 3.1. *XRD patterns and Raman scattering analyses*

XRD patterns of $MgNb_2O_6$ nanocrystals, ZnS nanocrystals and the ZnS/$MgNb_2O_6$ heterostructure, respectively.

**<Fig. 2(a–c)>**

XRD patterns indicate that all materials synthesized are a pure phase as shown in Fig. 2(a–c). Fig. 2(a) shows a structural evolution of the formation of the pure phase related to MN nanocrystals with the increase of calcination temperature (700 ºC to 1000 ºC). These materials possess a long-range structural order. All XRD peaks of MN crystals indicate that this material exhibits a columbite-type orthorhombic structure and space group (*Pbcn*) in good agreement with the JCPDS card 33-0875. The XRD peaks of ZnS nanocrystals, Fig. 2(b), indicate a sphalerite-type cubic structure and space group (F-43m) in good agreement with the JCPDS card 05-0566. Analysis of Fig. 2(c) and the shaper and broader XRD peaks points out the presence of ZnS/MN heterostructure.

It is well known that Raman spectroscopy is a suitable structural analytical technique used to the identification of traces at impurities (secondary phases), as well as changes in the structure, at a wide range of ceramic materials when XRD has not enough resolution. Spectroscopic techniques are sensitive to the short-range order showing a higher limit of detection, therefore much more appropriate to check traces of free niobium oxide in columbite powders and to investigate the degree of structural order-disorder at short-range in the materials. Fig. 3 (a-c) shows MR spectra collected at room temperature of the MN nanocrystals calcined at different temperatures, ZnS

nanocrystals and ZnS/MN heterostructure, respectively. Neither niobium chloride and magnesium acetate can be seen in the MR spectra of the MN nanocrystals calcined at 700 and 1000 °C (Fig. 3a and b), revealing that $NbCl_5$ has completely reacted with $Mg(OAc)_2$. This could be attributed to high reactivity of magnesium and niobium species. The spectra present typical bands corresponding to the normal vibration modes of $MgNb_2O_6$ [18]. Peaks centered at 847 and 905 $cm^{-1}$ can be indexed to the O-Nb-O stretching vibration mode. The MR spectrum of ZnS nanocrystals (Fig. 3(c)) is consistent with the previously reported results from Cheng et al. [19].

It is notable that the MR spectrum of the MN-700 °C exhibited broad vibrational modes, indicating structural disorder at short-range. In addition, the disorder structure in the MN was decreased when increased calcination temperature. This was a consequence of the enhancement in crystallinity of the columbite phase. The MR spectrum of the ZnS/MN-700 °C heterostructure did not present well-defined Raman peaks due to short-range disorder. However, this behavior was not observed in the ZnS/MN-1000 °C heterostructure, indicating a high degree of short-range structural order in the lattice.

**<Fig. 3(a–c)>**

### 3.2. *FEG-SEM images and EDX pattern analyses*

Typical FE-SEM images and EDX patterns of ZnS nanocrystals and ZnS/MN heterostructure samples with MN treated at different temperatures (700 ºC and 1000 ºC) are shown in the Fig. 4(a-c), respectively.

**<Fig. 4(a-c)>**

FE-SEM images shown in Fig. 4(a) indicate that MN crystals heat-treated at 700 ºC are covered by some of ZnS nanocrystals. Moreover, the MN nanocrystals have an agglomerated nature with diameter of approximately 100 nm because of the synthesis method. These $ZnS/MgNb_2O_6$ heterostructures exhibit the presence of the following chemical elements (Nb, Mg, Zn, S and O) as shown by the EDX spectrum. The amount of these elements depends on the selected area of the EDX analyses. The morphology of $ZnS/MgNb_2O_6$ heterostructures is substantially altered with the

increase of heat-treatment to 1000 ºC (Fig. 4(b)). The temperature raise promotes a major agglomeration of ZnS nanocrystals on the MN nanocrystals surface due to an increase in the overall diffusion rate during the sintering process. Finally, the ZnS nanocrystals are shown in Fig. 4(c), with a nearly-spherical shape; the average crystal size is in a range of 4 to 10 nm. These nanocrystals also have an agglomerate nature caused by high surface energy and Van der Waals forces. Fig. 4(c) shows the EDX pattern analysis which indicates the presence of Zn and S elements as the majority composition of ZnS nanocrystals.

### 3.4. *TEM and HR-TEM images analyses*

TEM images of ZnS/MN heterostructure samples with MN treated at different temperatures and ZnS nanocrystals are shown in the Fig. 5(a-d), respectively.

**<Fig. 5(a-d)>**

TEM images presented in Fig. 5(a) show the presence of several ZnS nanocrystals on the MN nanocrystal surfaces; some ZnS nanocrystals were diffused into the MN nanocrystals. The presence of these ZnS/$MgNb_2O_6$ heterostructures is best illustrated by means of the HR-TEM images in Fig. 5(b) and Fig. 5(c), respectively. More specifically, Fig. 5(b) the lower right inset shows the fringe spacing of 0.32 nm indexed to the (111) planes of spharelite ZnS. The ZnS nanocrystals remain in contact with the MN nanocrystals and the coalescence process takes place, resulting in the formation of irregular large morphologies of thousands of aggregated nanocrystals (Fig. 4(c)). The SAED analysis illustrated (inset) was obtained from Fig. 5(d) shows that the diffraction patterns 111, 220 and 311 planes, respectively, and confirmed that these ZnS nanocrystals present a single phase with a cubic structure and are in reasonable agreement with the complementary XRD data.

### 3.5. *UV–vis absorption spectroscopy analyses*

The optical band gap energy ($E_{gap}$) was calculated by the Kubelka and Munk method [20] which is based on the transformation of diffuse reflectance measurements to estimate $E_{gap}$ values with good accuracy within the limits of assumptions when they are modeled in three dimensions [21]. In

particular, it is useful in limited cases of an infinitely thick sample layer. The Kubelka–Munk equation for any wavelength is described by Eq. (1):

$$F(R_\infty) = \frac{(1-R_\infty)^2}{2R_\infty} = \frac{k}{s} \quad (1)$$

where $F(R_\infty)$ is the Kubelka–Munk function or absolute reflectance of the sample. In our case, magnesium oxide (MgO) was the standard sample in reflectance measurements. $R_\infty = R_{sample}/R_{MgO}$ ($R_\infty$ is the reflectance when the sample is infinitely thick), $k$ is the molar absorption coefficient, and $s$ is the scattering coefficient. In a parabolic band structure, the optical band gap and the absorption coefficient of semiconductor oxides [22] can be calculated by Eq. (2):

$$\alpha h\nu = C_1\left(h\nu - E_{gap}\right)^n \quad (2)$$

where $\alpha$ is the linear absorption coefficient of the material, $h\nu$ is the photon energy, $C_1$ is a proportionality constant, $E_{gap}$ is the optical band gap and $n$ is a constant associated with different kinds of electronic transitions ($n$ = 1/2 for a direct allowed, $n$ = 2 for an indirect allowed, $n$ = 1.5 for a direct forbidden and $n$ = 3 for an indirect forbidden). According to the literature [23], niobates and sulfides exhibit an optical absorption spectrum governed by direct electronic transitions. In this phenomenon, after the electronic absorption process, electrons located in maximum energy states in the valence band (VB) revert to minimum-energy states in the conduction band (CB) under the same point in the Brillouin zone. Based on this information, $E_{gap}$ values for $MgNb_2O_6$ nanocrystals, ZnS nanocrystals and ZnS/$MgNb_2O_6$ heterostructures were calculated using $n$ = 1/2 in Eq. 2. Finally, using the remission function described in Eq. 1 with $k = 2\alpha$, we obtain the modified Kubelka–Munk equation as indicated in Eq. (3):

$$[F(R_\infty)h\nu]^2 = C_1\left(h\nu - E_{gap}\right) \quad (3)$$

Therefore, finding the $F(R_\infty)$ value from Eq. (1) and plotting a graph of $[F(R_\infty)h\nu]^2$ against $h\nu$, we can determine $E_{gap}$ values for MN nanocrystals, ZnS nanocrystals and ZnS/$MgNb_2O_6$ heterostructures with greater accuracy by extrapolating the linear portion of UV-vis curves.

Fig. 6(a–e) show UV-vis spectra where we employed Eq. (3) by extrapolating the linear portion of UV-vis curves to calculate approximate $E_{gap}$ values of MN nanocrystals heat treated at 700 ºC

and 1000 ºC, the ZnS/MN-700 ºC heterostructure, the ZnS/MN-1000 ºC heterostructure and the ZnS nanocrystals, respectively.

**<Figs. 6(a–e)>**

In Fig. 6(a-e), distinct $E_{gap}$ values calculated from UV-vis spectra indicate the existence of intermediary energy levels within the optical band gap. These energy states are basically composed of O 2*p* orbitals near the valence band (VB) as well as Nb 4*d* orbitals and Mg 3*s* orbitals below the conduction band (CB). The origin of these energy levels as related to their respective molecular orbitals is directly related to structural order-disorder in the random lattice which is a consequence of a symmetry break between O–Mg–O, O–Nb–O bonds, (oxygen vacancies) and/or distortions on both octahedral $[MgO_6]$/$[NbO_6]$ clusters as well as tetrahedral $[ZnS_4]$ clusters [24]. Analysis of Fig. 2(a) shows that MN heat treated at 700 ºC has broad XRD peaks, which is characteristic of presence of pure MN nanocrystals with high $E_{gap}$ values (4.15 eV). The increase of thermal treatment to 1000 ºC can remove the large majority of surface defects found at 700 ºC. However, the structural defects at medium range still remain due to presence of distortions on octahedral $[MgO_6]$/$[MgO_6]$ clusters which promotes a reduction $E_{gap}$ values (4.06 eV). Fig. 6(c,d) shows a decrease in both $E_{gap}$ values (4.06 eV and 3.55 eV) for the ZnS/MN-700 ºC heterostructure and the ZnS/MN-1000 ºC heterostructure. This result indicates a synergistic effect of a mixture of electronic levels and orbitals rising from the orthorhombic structure of MN crystals and cubic structure of ZnS nanocrystals with low $E_{gap}$ values (3.48 eV) shown in Fig. 6(e).

### 3.6. *PL emission analyses*

Fig. 7 shows the PL emission of MN-700 ºC nanocrystals, MN-1000 ºC nanocrystals, the ZnS/MN-700 ºC heterostructure, the ZnS/MN-1000 ºC heterostructure and ZnS nanocrystals, respectively.

**<Figs. 7>**

According Zhou et al. [25], PL emission of $MgNb_2O_6$ powders is related to a charge transfer band from $Nb^{5+}$ ions to $O^{2-}$ ions near 257 nm. Moreover, these authors state that their MN powders prepared by the solid state reaction method have a low intensity of luminescence emission at room temperature. Other researchers [26], report that the visible PL emission band for MN:$Ni^{2+}$ crystals at 26 K is located at 527 nm. However, these crystals have a PL emission ten times lower at ambient temperature and attributed this optical behavior to a multiphonon sideband characteristic of a $^1T_3 \rightarrow {}^3A_2$ transitions. Polgár et al. [27] have obtained MN single crystals by the Czochralski method and attributed that their PL emission maximum near 530 nm is related to an oxygen deficiency. Fang et al. [28] report, that MN nanocrystals exhibit a broad and strong blue PL emission band maximum at 450 nm which they ascribed to the self-activated niobate octahedra group $[NbO_6]^{-7}$. Some authors [29] have proposed that the PL properties of ZnS nanocrystals can be asssociated to surface defects. Other researchers [30-31] relate the PL emission in ZnS nanocrystals to the presence of sulfur vacancy and point defects.

The PL behavior can be explained by the presence of photogenerated electron-hole pair (excitons) processes and in terms of the electronic transitions between the VB and CB. In this paper, we explain that PL properties of MN nanocrystals and ZnS nanocrystals and ZnS/MN heterostructures are related to structural defects at medium range present in the lattices of orthorhombic, cubic and orthorhombic/cubic heterostructures. The distortions on octahedral $[MgO_6]$/$[NbO_6]$ clusters in MN nanocrystals, tetrahedral $[ZnS_4]$/$[ZnS_3V_s^x]$ clusters, and octahedral/tetrahedral $[MgO_6]$/$[ZnS_4]$ clusters and octahedral/tetrahedral $[NbO_6]$/$[ZnS_4]$ clusters are due to lattice-mismatched heterostructures. Therefore, based in our experimental results of XRD patterns (Fig. 2(a–c)) and the change in $E_{gap}$ values (Fig. 6(a–e)), we can attribute the presence of structural defects in the lattice and electronic structure of pure crystals and heterostructures. Morphological aspects are able to dislocate crystal lattice planes as well as adjacent particles in aggregates which produce defects in crystals. Therefore, these crystals (ZnS/MN) have favorable conditions to promote the charge transfer process from distorted $[NbO_6]_d$ or $[MgO_6]_d$ clusters to undistorted $[NbO_6]_o$ , $[MgO_6]_o$ or

$[ZnS_4]_o$ and $[ZnS_3V_s^x]$ complex vacancies clusters and to $[ZnS_4]^x$ clusters. Other factors can also be involved in this case such as the degree of orientation between surface defects. All these factors have an influence in the intensity of the PL emission.

In this particular case of MN nanocrystals heat treated at 700 ºC and 1000 ºC a low PL emission is observed, while ZnS nanocrystals have an intense PL emission at room temperature (Fig. 7). In addition, we can verify that the ZnS/MN-700 ºC and 1000 ºC heterostructures have a high intense PL emission with a displacement from 489 nm (blue region) to 515 nm (green region). Therefore, a synergistic effect takes place which significantly improves the optical properties (Fig. 7) of the as-synthetized ZnS/MN heterostructures. The main difference in PL spectra of ZnS nanocrystals can be attributed to the ratio between the interface $[NbO_6]_o$ / $[MgO_6]_o$ clusters and disorder/vacancies in $[NbO_6]_d$ , $[MgO_6]_d$ and $[ZnS_3V_s^x]$ clusters. The order-disorder effect or structural distortions remaining in the lattice promote a constant electronic charge transfer between ordered (o) and disordered (d) vacancy ($V_s^x$) clusters, which is possible according to equations 5-11:

$$[MgO_6]_o^x + [MgO_6]_d^x \Rightarrow [MgO_6]_o^{'} + [MgO_6]_d^{\cdot} \quad (5)$$

$$[NbO_6]_o^x + [NbO_6]_d^x \Rightarrow [NbO_6]_o^{'} + [NbO_6]_d^{\cdot} \quad (6)$$

$$[NbO_6]_o^x + [MgO_6]_d^x \Rightarrow [NbO_6]_o^{'} + [MgO_6]_d^{\cdot} \quad (7)$$

$$[MgO_6]_o^x + [NbO_6]_d^x \Rightarrow [MgO_6]_o^{'} + [NbO_6]_d^{\cdot} \quad (8)$$

$$[ZnS_4]_o^x + [ZnS_3V_s^x] \Rightarrow [ZnS_4]_o^{'} + [ZnS_3V_s^{\cdot}] \quad (9)$$

$$[MgO_6]_o^x + [ZnS_3V_s^x] \Rightarrow [MgO_6]_o^{'} + [ZnS_3V_s^{\cdot}] \quad (10)$$

$$[NbO_6]_o^x + [ZnS_3V_s^x] \Rightarrow [NbO_6]_o^{'} + [ZnS_3V_s^{\cdot}] \quad (11)$$

The equations (5-11) represent the possible cluster-to-cluster charge transfer mechanisms involving electronic transitions and recombination processes between clusters in an MN nanocrystal, ZnS nanocrystals and ZnS/MN heterostructures. We believe that these structural

defects are due to symmetry breaking processes between the clusters at medium range, promoting the formation of intermediate levels between the VB and CB, which decrease the band gap, and consequently an improvement in PL emission properties at room temperature (Fig. 7).

## 4. Conclusions

In summary, we have successfully obtained MN crystals by the coprecipitation/calcination method at 700 ºC and 1000 ºC, while ZnS nanocrystals and ZnS/MN heterostructures have been synthetized by means of the MAH method. XRD patterns and MR spectra confirmed that the MN nanocrystals have a columbite-type orthorhombic structure and space group (Pbcn); ZnS nanocrystals have a sphalerite-type cubic structure and space group (F-43m) and ZnS/MN heterostructures have both structures. FE-SEM images show that ZnS/MN heterostructures have irregular morphologies, non-uniform particle size distribution, and an agglomerated nature. TEM and HR-TEM images proved that the ZnS nanocrystals are located on the surface of MN nanocrystals. An analysis of the UV-vis spectra indicates the presence of intermediary levels between the VB and CB of ZnS/MN heterostructures and a reduction of $E_{gap}$ values. Finally, an improvement of optical properties and a displacement of the PL band emission to the green region were observed for ZnS/MN heterostructures, and a plausible mechanism for a relationship between optical properties and order-disorder effects is proposed.

***Acknowledgments***

The authors gratefully acknowledge the support of the Brazilian agencies CNPq/INCTMN (152892/2012-5), FAPESP (CEPID-CDMF2013/07296-2) and CAPES. J. Andrés acknowledges the Generalitat Valenciana (Prometeo/2009/053 project), the Ministerio de Economía y Competitividad, Spain (project CTQ-2012-36253-C03-02), the Programa de Cooperación Científica con Iberoamerica (Brazil) and Ministerio de Educació, Cultura y Deporte (PHB2009-0065 project).

**References**

[1] R.C. Pullar, K. Okeneme, N. McN. Alford, Temperature compensated niobate microwave ceramics with the columbite structure, $M^{2+}Nb_2O_6$, *J. Eur. Ceram. Soc*. **23** (2003) 2479–2483.

[2] L.P.S. Santos, E.R. Camargo, M.T. Fabbro, E. Longo, E.R. Leite, Wet-chemical synthesis of magnesium niobate nanopowders, *Ceram. Int.,* **33** (2007) 1205-1209.

[3] L.P.S. Santos, E. Longo, E.R. Leite, E.R Camargo, Combined wet-chemical process to synthesize 65PMN-35PT nanosized powders. *J. Alloys. Compd*. **372** (2004) 111-115.

[4] J.V. Hanna, K.J. Pike, T. Charpentier, T.F. Kemp, M.E. Smith, B.E.G. Lucier, R.W. Schurko, L.S. Cahill, A $^{93}$Nb solid-State NMR and density functional theory study of four- and six-coordinate niobate systems, *Chem. Eur. J.* **16** (2010) 3222–3239.

[5] C.H. Hsu, C.F. Tseng, C.L. Huang, Microwave Dielectric Properties of $MgNb_2O_6$ Ceramics with $Fe_2O_3$ Additives, *Jpn. J. Appl. Phys.* **44** (2005) 8043–8047.

[6] L. Li, G. Feng, D. Wang, H. Yang, Z. Gao, B. Li, D. Xu, Z. Ding, X. Liu, Optical floating zone method growth and photoluminescence property of $MgNb_2O_6$ crystal, *J. Alloys Compd.* **509** (2011) L263–L266.

[7] C. Zaldo, M.J. Martin, C. Coya, K. Polgár, A. Péter, J. Paitz, Optical properties of $MgNb_2O_6$ single crystals: a comparison with $LiNbO_3$, *J. Phys.: Condens. Matter.* **7** (1995) 2249-2257.

[8] P. Kumbhakar, M. Chattopadhyay, A.K. Mitra, Nonlinear optical properties of doped ZnS quantum dots, *Inter. J. Nanosci*. **10** (2011) 177-180.

[9] F.A. La Porta, M.M. Ferrer, Y.V.B. de Santana, C.W. Raubach, V.M. Longo, J.R. Sambrano, E. Longo, J. Andrés, M. Siu Li, J.A. Varela, Synthesis of wurtzite ZnS nanoparticles using the microwave assisted solvothermal method, *J. Alloys Compd*. **556** (2013) 153–159.

[10] Y.V.B. de Santana, C.W. Raubach, M.M. Ferrer, F. La Porta, J.R. Sambrano, V.M. Longo, E.R. Leite, E. Longo, Experimental and theoretical studies on the enhanced photoluminescence activity of zinc sulfide with a capping agent, *J. Appl. Phys.* **110** (2011) 123507–123513.

[11] C.W. Raubach, Y.V.B. Santana, M.M. Ferrer, V.M. Longo, J.A. Varela, W. Avansi Jr., P.G.C. Buzolin, J.R. Sambrano, E. Longo, Strutural and optical approach of CdS@ZnS core–shell system,*Chem. Phys. Lett.* **536** (2012) 96-99.

[12] L.S. Cavalcante, M.F.C. Gurgel, A.Z. Simes, E. Longo, J.A. Varela, M.R. Joya, P.S. Pisani, Intense visible photoluminescence in Ba(Zr0.25Ti0.75)*O*3 thin films, *Appl. Phys. Lett.* **90** (2007) 011901.

[13] L. Wang, H.W. Wei, Y.J. Fan, X.Z. Liu, J.H. Zhan, Synthesis, Optical Properties, and Photocatalytic Activity of One-Dimensional CdS@ZnS Core-Shell Nanocomposites, *Nanoscale Res. Lett.* **4** (2009) 558-564.

[14] M.J.L. Santos, J. Ferreira, E. Radovanovic, R. Romano, O.L. Alves, E.M. Girotto,

Enhancement of the photoelectrochemical response of poly(terthiophenes) by CdS(ZnS) core-shell nanoparticles, *Thin Solid Films* **517** (2009) 5523-5529.

[15] A. Ishizumi, Y. Kanemitsu, Luminescence Spectra and Dynamics of Mn-Doped CdS Core/Shell Nanocrystals, *Adv. Mater.* **18** (2006) 1083-1085.

[16] E. Papulovskiy, A.A. Shubin, V.V. Terskikh, C.J. Pickard, O.B. Lapina, Theoretical and experimental insights into applicability of solid-state 93Nb NMR in catalysis, *Phys. Chem. Chem. Phys.* **15** (2013) 5115–5131.

[17] R.L. Withers, T.R. Welberry, A. Pring, C. Tenailleau, Y. Liu, 'Soft' phonon modes, structured diffuse scattering and the crystal chemistry of Fe-bearing sphalerites, *J. Solid State Chem.* **178** (2005) 655-660.

[18] E. Husson, Y. Repelin, N.Q. Dao, H. Brusset, Normal coordinate analysis of the $MNb_2O_6$ series of columbite structure (M = Mg, Ca, Mn, Fe, Co, Ni, Cu, Zn, Cd), *J. Chem. Phys.* **67** (1977) 1157-1163.

[19] Y.C. Cheng, C.Q. Jin, F. Gao, X.L. Wu, W. Zhong, S.H. Li, P.K. Chu, Raman scattering study of zinc blend and wurtzite ZnS, *J. Appl. Phys.* **106**, 123505 (2009) 1-5.

[20] P. Kubelka, F. Munk-Aussig, Ein Beitrag zur Optik der Farban striche, Zeit. Für. Tech. Physik. **12** (1931) 593–601.

[21] A.E. Morales, E.S. Mora, Use of diffuse reflectance spectroscopy for optical characterization of un-supported nanostructures, U. Pal, Rev. Mex. Fis. S. **53**, (2007) 18–22.

[22] R.A. Smith, Semiconductors, second ed.; Cambridge University Press: London, 1978.

[23] C. Thierfelder, S. Sanna, Arno Schindlmayr, and W. G. Schmidt, Do we know the band gap of lithium niobate?, *Phys. Status Solidi* C. **7** (2010) 362–365.

[24] O.I. Velikokhatnyi, K. Kadakia, S.K. Park, P.N. Kumta, Theoretical Study of Magnesium and Zinc Tantalates and Niobates as Prospective Catalyst Supports for Water Eletrolysis, *J. Electrochem. Soc*. **159** (2012) F607-F616.

[25] L. Zhou, J. Huang, F. Mo, Preparation and photoluminescence properties of $MgNb_2O_6$:$Eu^{3+}$, $Bi^{3+}$ red-emitting phosphor, *Mater. Sci. Poland*. **32** (2014) 88-92.

[26] P. McBride, R. Sherlock, T.J. Glynn, G. Walker, Optical spectroscopy of $MgNb_2O_6$ and $ZnNb_2O_6$ doped with $Ni^{2+}$, *J. Appl. Spectrosc*. **62** (1995) 636–642.

[27] K. Polgár, A. Péter, J. Paitz, C. Zaldo, Crystal growth and preparation of colourless $MgNb_20_6$ single crystals, *J. Crys. Growth*. **151** (1995) 365-368.

[28] T.H. Fang, Y.J. Hsiao, Y.S. Chang, L.W. Ji, S.H. Kang, Luminescent and structural properties of $MgNb_2O_6$ nanocrystals, *Curr. Opin. Solid State Mater. Sci*. **12** (2008) 51–54.

[29] N. Kumbhojkar, V.V. Nikesh, A. Kshirsagar, S. Mahamunia, Photophysical properties of ZnS nanoclusters, *J. Appl. Phys*. **88** (2000) 6260–6264.

[30] R. Viswanath, H.S.B. Naik, Y.K.G. Somalanaik, P.K.P. Neelanjeneallu, K.N. Harish, M.C. Prabhakara, Studies on characterization, optical absorption, and photoluminescence of yttrium doped ZnS nanoparticles, *J. Nanotechnol*. **2014** (2014) 924797–924804.

[31] S. Lee, D. Song, D. Kim, J. Lee, S. Kim, I.Y. Park, Y.D. Choi, Effects of synthesis temperature on particle size/shape and photoluminescence characteristics of ZnS:Cu nanocrystals," *Mater. Lett*. **58** (2004) 342–346.

**Figures:**

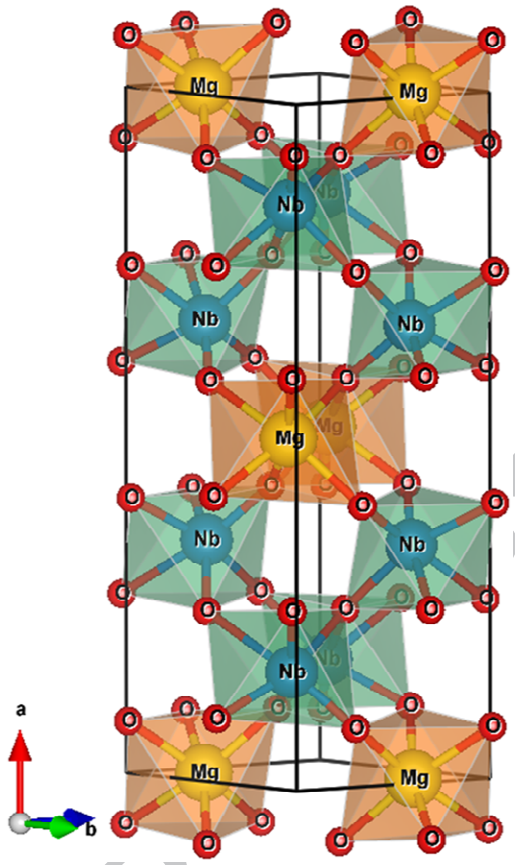


**(a)**

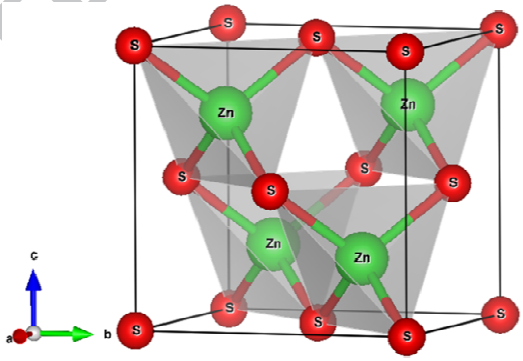


**(b)**

**<Fig. 1(a, b)>**

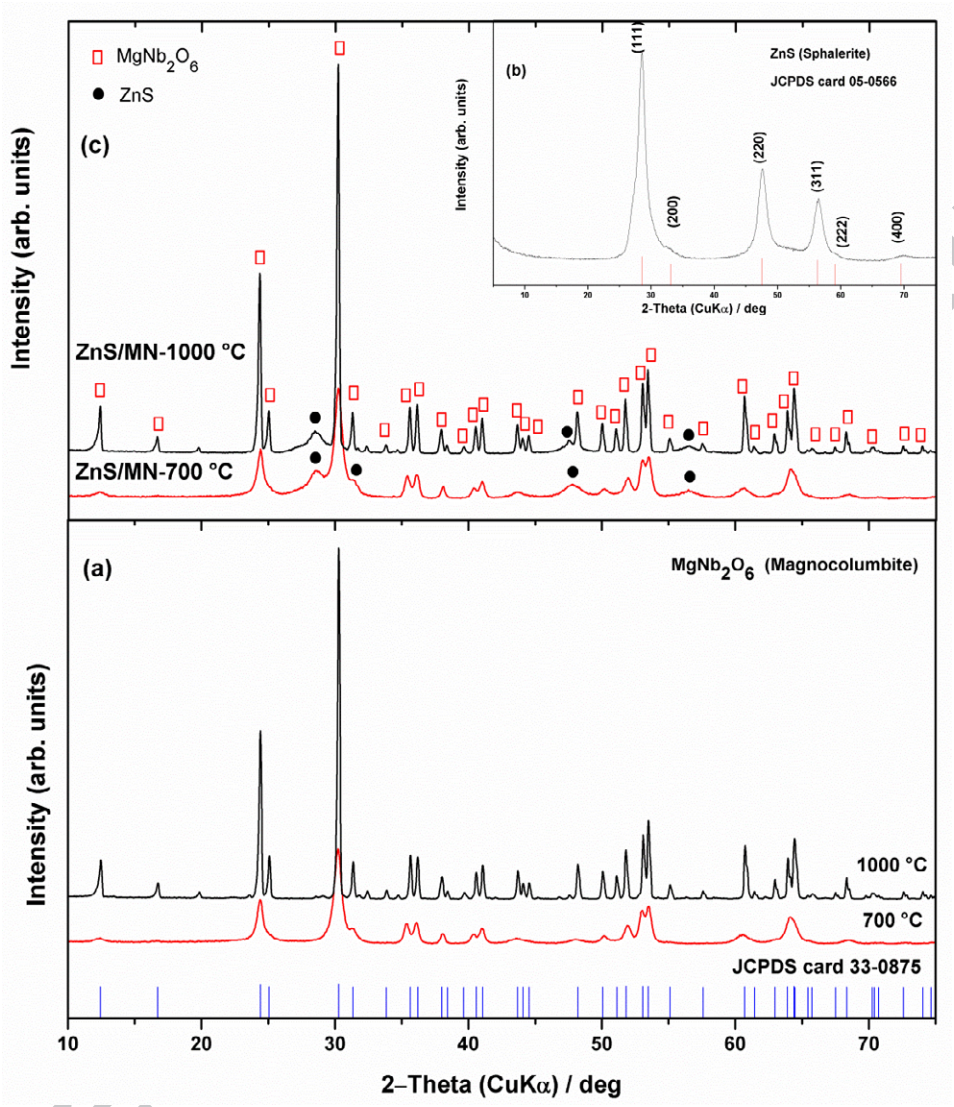


**<Figs. 2(a-c)>**

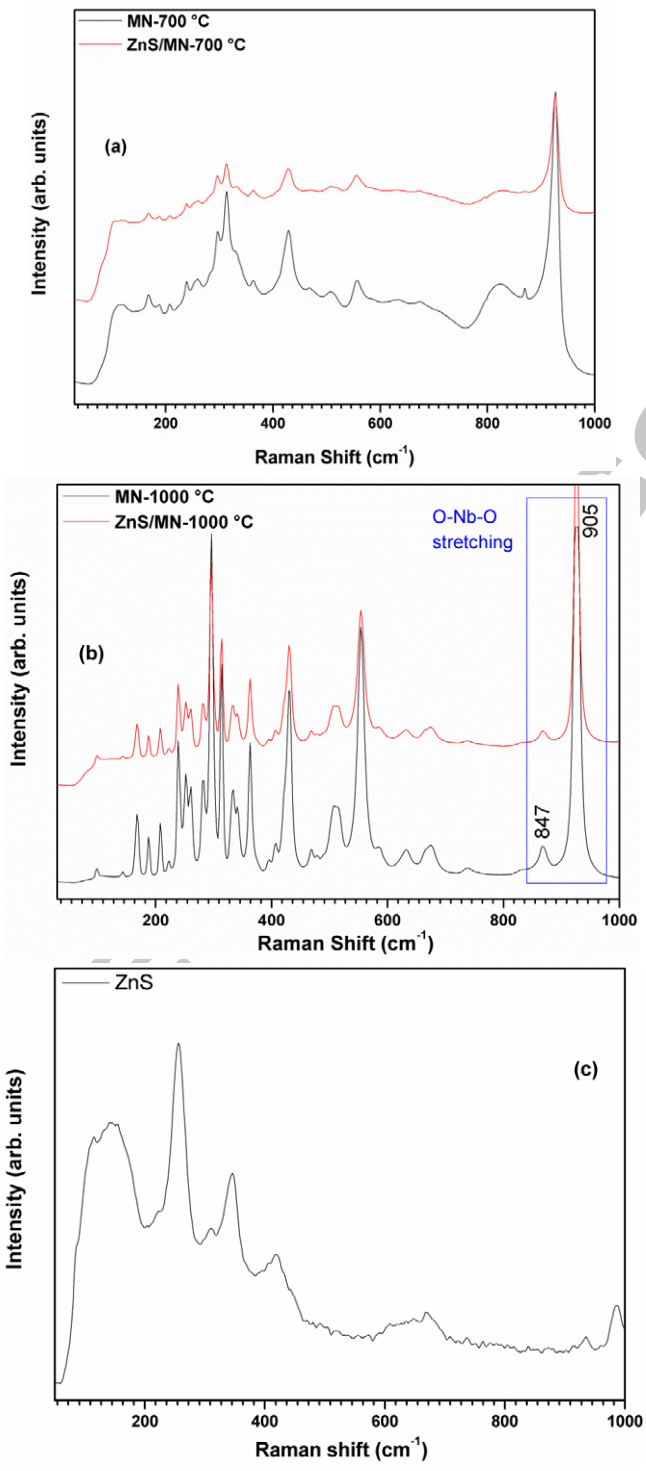


**<Figs. 3(a-c)>**

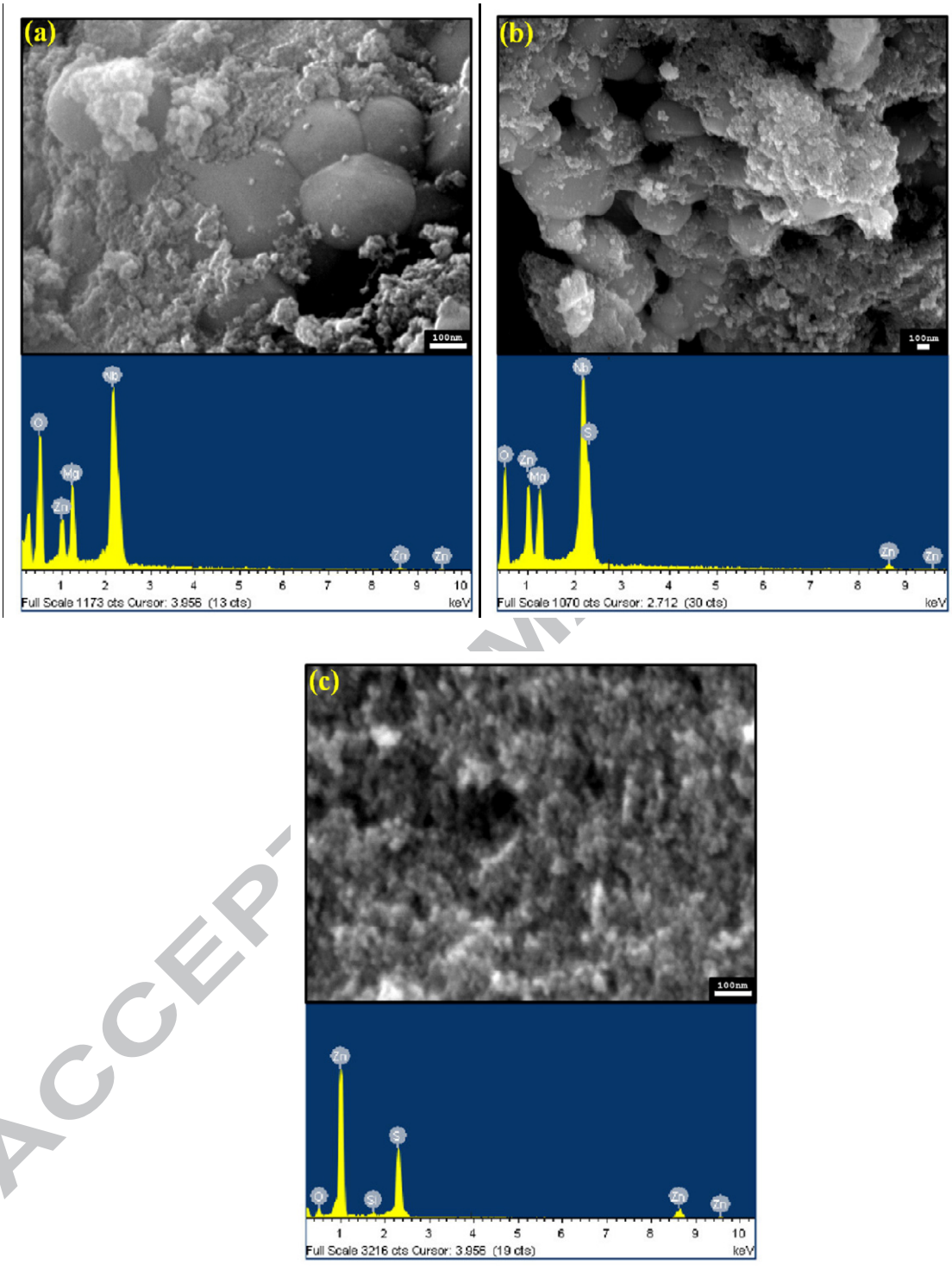
(a)
100nm
O
Mg
Zn
Zn
Zn
1 2 3 4 5 6 7 8 9 10
Full Scale 1173 cts Cursor: 3.956 (13 cts)
keV
(b)
100nm
Mg
S
O
Zn
Mg
Zn
Zn
1 2 3 4 5 6 7 8 9
Full Scale 1070 cts Cursor: 2.712 (30 cts)
keV
(c)
100nm
Zn
S
O
Si
Zn
Zn
1 2 3 4 5 6 7 8 9 10
Full Scale 3216 cts Cursor: 3.956 (19 cts)
keV

**<Figure 4(a-c)>**

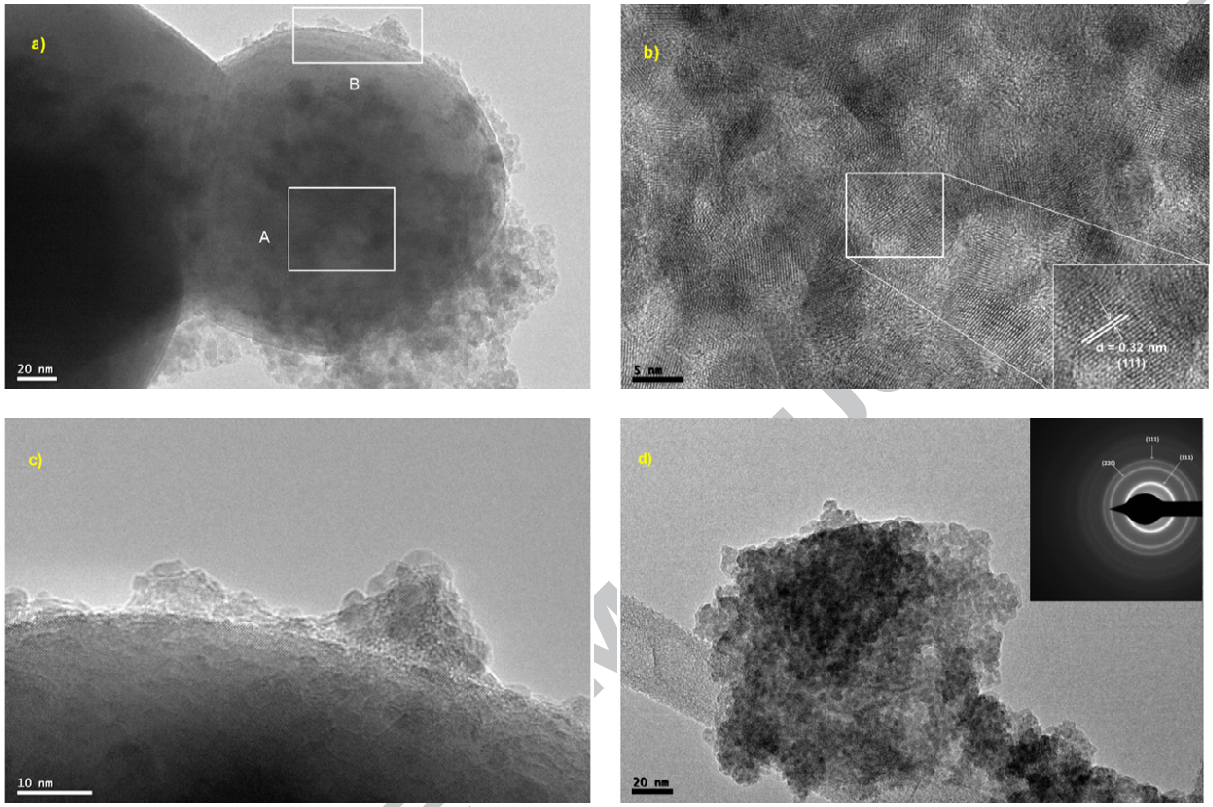


**<Figs. 5(a–d)>**

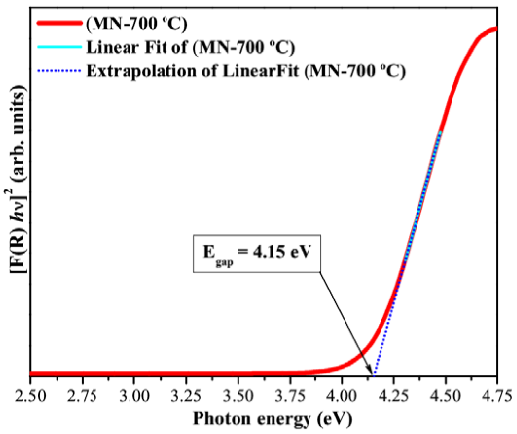


(a)

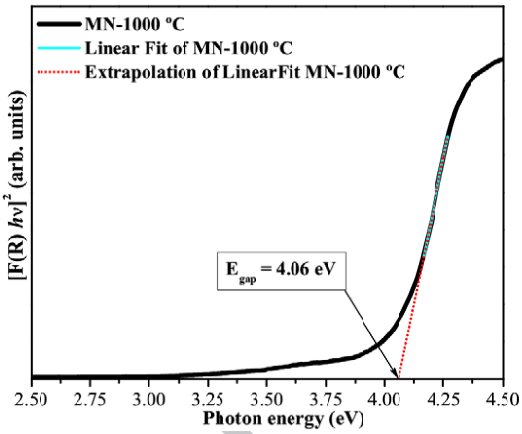


(b)

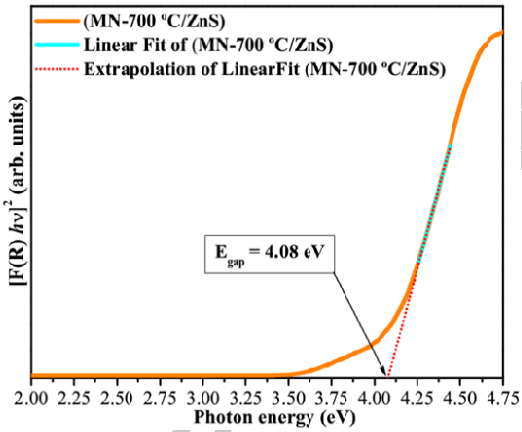


(c)

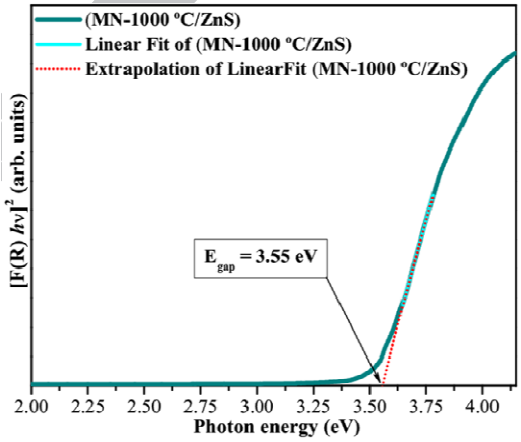


(d)

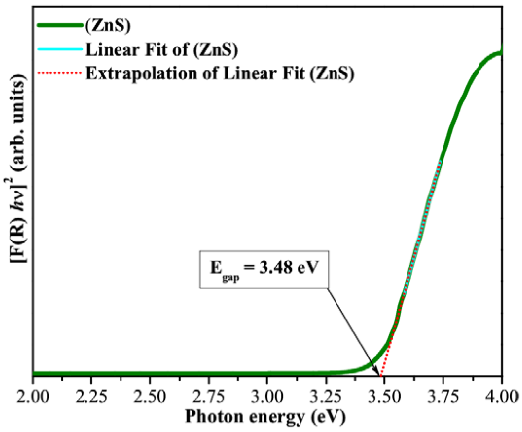


(e)

**<Fig. 6(a-e)>**

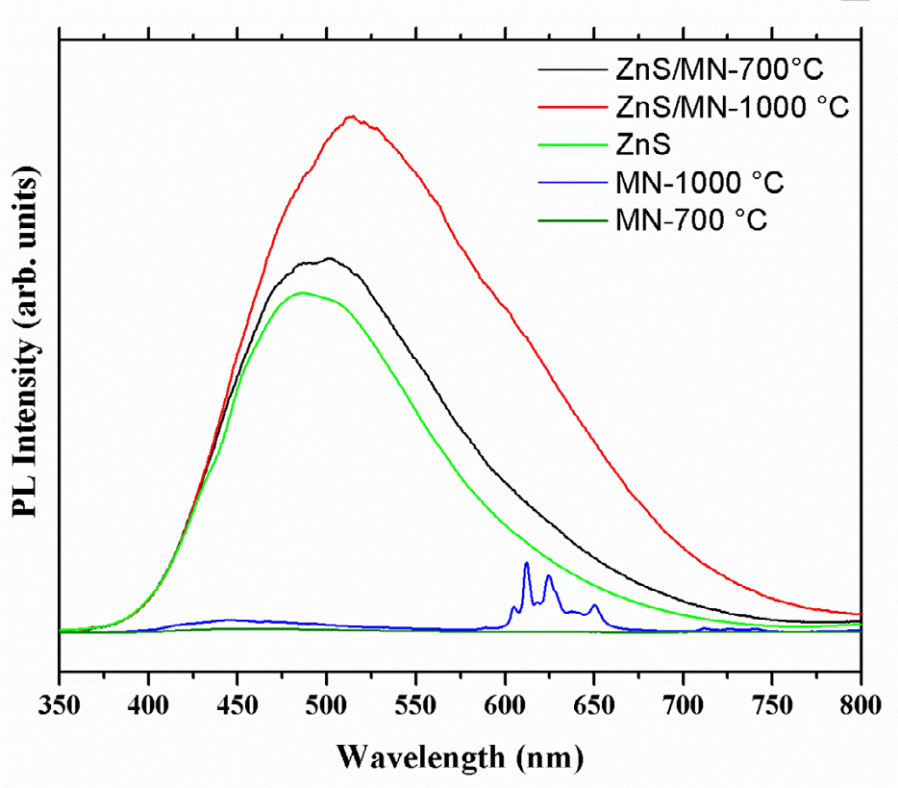


**<Fig. 7>**

**Figure Captions**

**Figure 1.** Schematic representation of the unit cells. (a) $MgNb_2O_6$ crystal; (b) ZnS crystal.

**Figure 2.** XRD patterns from (a) $MgNb_2O_6$ columbite phase obtained at diferente temperatures for 1h with heating and cooling rates of 10 °C $min^{-1}$; (b) ZnS pure and the corresponding JCPDS standard; (c) ZnS/MN heterostructures.

**Figure 3.** Micro-Raman spectra of the (a) MN-700 °C and ZnS/MN-700 °C heterostructure; (b) MN-1000 °C and ZnS/MN-1000 °C heterostructure; (c) ZnS pure, respectively.

**Figure 4.** FE-SEM images and EDX patterns of (a) ZnS/MN-700 °C; (b) ZnS/MN-1000 °C and (c) ZnS in FEG-SEM images.

**Figure 5.** a) TEM image of ZnS/MN-1000 °C; (b) HR-TEM image of region A; (c) HRTEM image of region B; (d) TEM image of ZnS pure. The inset in (d) shows the SAED pattern of ZnS.

**Figure 6.** UV-vis spectra of the (a) MN-700 °C; (b) MN-1000 °C; (c) ZnS/MN-700 °C; (d) ZnS/MN-1000 °C and (e) ZnS pure.

**Figure 7.** The PL spectra of MN-700 °C, MN-1000 °C powders, ZnS/MN-700 °C, ZnS/MN-1000 °C heterostructures and ZnS nanocrystals at room temperature.

## Graphical Abstract:

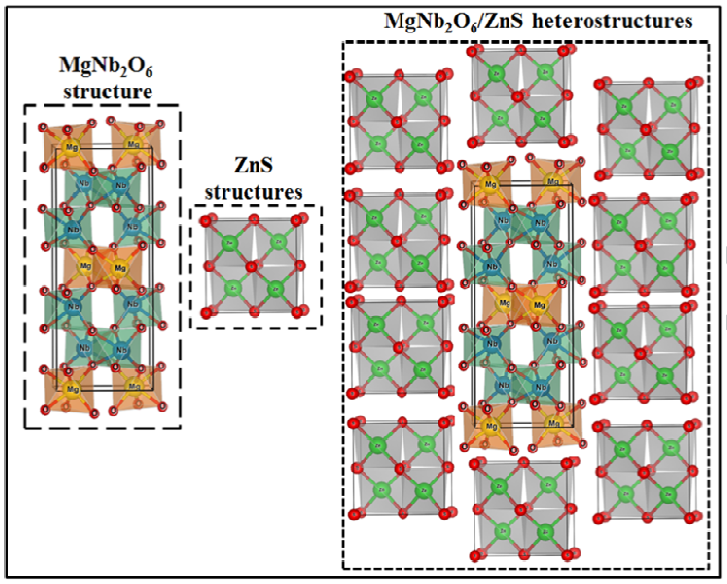


**Highlights**

- $ZnS/MgNb_2O_6$ heterostructures were obtained by copreciptation/calcination method and a microwave assisted hydrothermal method combined.
- The ZnS nanocrystals indicate a sphalerite-type cubic structure and $MgNb_2O_6$ nanocrystals indicate a columbite-type structure.
- $ZnS/MgNb_2O_6$ heterostructures showed photoluminescence properties.
- Photoluminescence emission is related to structural defects at medium range present in the lattice of orthorhombic, cubic and orthorhombic/cubic heterostructures.